Supplementary Information for

Functional and structural diversification of incomplete phosphotransferase system and associated components in cellulose-degrading clostridia

by
Tao Xu et al.

Supplementary text A

On soluble carbon mix (CM, consisting of cellobiose, glucose, arabinose, and xylose), which mimics the co-presence of diverse sugars released during lignocellulose biodegradation, the hprKi knockdown increased the maximal cell biomass and growth rate compared to the pRNAi control (**Figure 2B; Figure S2B**). In contrast, Δ*cph* and *cph*_S46D mutants decreased both cell biomass and growth rate. For carbohydrate utilization, the hprKi knockdown significantly reduced the consumption rate of cellobiose, xylose, and glucose (**Figure 2B**), and consequently had less sugars utilized during microbial fermentation (**Figure S2B**), suggesting a positive role for HprK in soluble carbon utilization. Although Δ*cph* and *cph*_S46D mutants significantly reduced the use of arabinose, xylose, and glucose, when compared to the parent strain, Δ*cph* presented a stronger effect than *cph*_S46D on decreasing pentose utilization (xylose and arabinose), indicating the involvement of Cph in pentose metabolism. However, Δ*cph* and *cph*_S46D presented an opposite effect on cellobiose utilization where Δ*cph* increased rather than decreased cellobiose utilization (**Figure 2B; Figure S2B**). These results suggest sugar type-specific regulatory mechanisms are mediated through Cph. Phenotypic changes in Δ*cph* and hprKi mutants also suggest that both Cph and HprK play a positive role in the metabolism of monosaccharides but differ in their impact on the polygenic trait of cell growth.

Studies on the most similar *ccpA*-like genes in *R. cellulolyticum* revealed that although both Δ*ccpA* and Δ*ccpB* mutants did not significantly affect cell biomass yield and growth rate (**Figure 2B**), they differed in the utilization of soluble sugars. Δ*ccpA* had no impact on the use of all soluble sugars tested here (**Figure 2B**); whereas Δ*ccpB* reduced the use of cellobiose and xylose and enhanced arabinose utilization. Therefore, these two *ccpA*-like transcriptional regulators have diverged functions and CcpB rather than CcpA is involved in the regulation of soluble sugar utilization.

As components of PTSs, such as HPr and CcpA, regulate transcription [1–3], we performed microarray-based transcriptomic analyses for Δ*cph*, Δ*ccpA*, and Δ*ccpB* on different carbon sources (**Figure 3A**). In general, all mutants presented many more differentially expressed genes (DEGs) when grown on carbon mix than on cellobiose (**Figure 3B; Figure S3A**). We then mainly focused on DEGs in each mutant grown with carbon mix. Compared to the parent strain, *Δcph* had broad transcriptional changes in 286 genes (8.5% genes in the genome), which were enriched for diverse basic cellular functions (e.g., amino acid/protein biosynthesis, DNA/RNA metabolism and binding) and carbohydrate metabolism (**Table S2**). This suggests that this H15-free Cph is associated with pleiotropic functions, not limited to carbohydrate utilization. At the gene level, Δ*cph* significantly down-regulated genes involved in pentose phosphate pathway (Ccel_3191 & Ccel_3192), but up-regulated genes for cellobiose uptake (Ccel_2110) and glycosyl groups transferring (Ccel_0388, Ccel_0414, Ccel_2184, and Ccel_2987). These carbohydrate-associated transcriptional changes are in line with observed metabolic phenotypes in Δ*cph* - a decrease in penose utilization and an increase in cellobiose use (**Figure 2B**).

The *cph*_S46D mutant, carrying a point mutation at S46 in Cph to mimic the phosphorylation status, changed the transcription of 60 genes, 75% of which were downregulated and 30% of which overlapped with DEGs in Δ*cph* (**Table S2**). Down-regulation of the *cuaA* gene (Ccel_2112, a 2.5-fold decrease), which is indispensable for sensing and transporting cellobiose in *R. cellulolyticum* [4], could explain the reduced consumption of cellobiose in *cph*_S46D. It is also notable that downregulation of pentose phosphate pathway genes (Ccel_3191 and Ccel_3192) observed in Δ*cph*, became not significant in *cph*_S46D. These results suggest that S46D in Cph or phosphorylation at S46 in Cph is less likely to suppress pentose utilization through transcriptional regulation, but it indeed transcriptionally regulates cellobiose metabolism.

Transcriptional analysis revealed that when compared to the parent strain, Δ*ccpB* presented 239 DEGs on carbon mix versus 10 DEGs observed in Δ*ccpA* (**Figure 3B; Table S2**). Although no GO terms were significantly enriched by DEGs in Δ*ccpB*, these DEGs were involved in a variety of basic biological processes (e.g., carbohydrate metabolic process, DNA/RNA metabolism, ion binding, transporter activity, and amino acid or pyrimidine/purine

biosynthesis) (**Table S2**). This broad regulatory function of CcpB is in line with its metabolic importance to soluble sugars and functionally similar to reported CcpA in *B. subtilis* and *Staphylococcus mutans* [5, 6]. Previous studies have demonstrated that HPr interacts with CcpA and thereby modulates the DNA binding affinity of CcpA [2, 7–10]. Although there were more than 200 DEGs in *Δcph* and *ΔccpB* respectively (**Table S2**), only 71 genes (30% in Δ*ccpB* DEGs and 25% in Δ*cph* DEGs) were shared and enriched for some biological processes (e.g., monocarboxylic acid biosynthetic process, ATPase-coupled transmembrane transporter activity and quorum sensing) (**Figure S3B**). Plus differential catabolic and phenotypic features as shown above (**Figure 2B**), it seems that Cph and CcpB regulate transcription mainly through independent pathways.

Supplementary text B

Based on the canonical CCR mechanism, previous studies [11, 12] believed that inactivation of *ccpA* or *cph* could eliminate the repression caused by "cellobiose" in *R. cellulolyticum*, and therefore enhance the cellulose degradation efficiency as the repression expression of *cip-cel* operon caused by "cellobiose" would be released. In addition, a similar strategy for inactivation of *ccpA* has been successfully applied in *C. acetobutylicum*, in which the inactivation of CcpA in *C. acetobutylicum* could eliminate the glucose repression for xylose [13]. However, not to mention to increase the expression of the *cip-cel* gene operon or improve the cellulose degradation efficiency, inactivation of *cph* or *ccpA* caused the growth deficiency of *R. cellulolyticum*. Based on our incubation experiment (**Figure S3C**), we found that Cph and CcpA are indispensable to sustain a long-term high expression of the *cip-cel* gene cluster in *R. cellulolyticum*, especially for *cipC* (Ccel_0728), *cel48F* (Ccel_0729), and *cel9E* (Ccel_0732) (**Figure 3G**). All of these indicated that "canonical" CCR in *Firmicutes* does not apply for the *R. cellulolyticum* grown on cellulose. Considering the conserved 15His has been replaced by 15Asp in Cph, the major way for Cph in regulating carbon catabolism should be accomplished through protein-protein interaction instead of phosphoryl transference. Based on the IP-MS experiment for Cph (**Table S4 & Figure 4**), we found that Cph could potentially interact with some ribosomal proteins, the anti-sigma factor antagonist and the transcription termination factor Rho. Previous studies found that the transcript abundance of *cip-cel* operon can be attributed to site-specific RNA processing/stabilization; alternative sigma factor 24 and anti-sigma factors were

involved in regulating the expression of cellulosomal genes in clostridia [14, 15]. As a likely result, the Cph may influence the stabilization and abundance of *cip-cel* transcript through interacting with above proteins and finally inactivation of *cph* may not maintain the high expression of the *cip-cel* operon as we observed in the incubation experiment (**Figure 3G**). Genes encoding sigma factor 24 (Ccel_3319 & Ccel_1490) and anti-sigma-factor antagonist (Ccel_2286) were decreased by at least two fold in Δ*cph*. In addition to potentially binding to the RNA processing proteins, Cph was found to potentially interact with Cel9E (**Table S4**), suggesting unknown mechanisms may be involved in maintaining the high expression of the *cip-cel* operon. Although the CcpA was not found to interact with Cph or other HPr homologs in *R. cellulolyticum* as canonical CcpA did in *Bacillus*, inactivation of *ccpA* could also cause the collapse of high expression of *cip-cel* operon and down-regulation of genes encoding sigma factor 24 (Ccel_0927 and Ccel_1490). As a transcriptional factor, the CcpA could not bind to the nearby region of *cip-cel* operon including upstream, downstream or within the *cip-cel* operon from the ChIP-seq experiment (**Figure S4A and Table S3**). In addition, we did not observe that CcpA can bind to any RNAs through RNA immunoprecipitation assay. Finally, based on the IP-MS experiment (**Table S4)**, those potential interaction proteins for CcpA did not have a reasonable explanation to explain the regulation of *cip-cel* gene operon by CcpA. Therefore, all of these indicated that CcpA must indirectly regulate the expression of the *cip-cel* operon through complicated alternative ways. Based on the ChIP-seq result and microarray analysis (**Figure S4A**; **Table S2 and S3**), we found the CcpA may directly regulate the expression of a FGGY-family carbohydrate kinase (Ccel_1006). Coincidentally, a recent study found that HPr could interact with a carbohydrate kinase and regulate the activity of the carbohydrate kinase [16]. Therefore, there may be a special link instead of direct protein-protein interaction among CcpA, Cph, and that FGGY-family carbohydrate kinase (e.g. phosphorylated sugar by the carbohydrate kinase as ligand to regulate CcpA, CcpA could regulate the expression of the carbohydrate kinase and Cph could regulate the activity of the carbohydrate kinase). In addition to that, other complicated mechanisms including distal regulation might also be involved in regulating the maintenance of *cip-cel* gene operon expression through CcpA. Further study is needed to find out how CcpA maintained the high expression of the *cip-cel* operon.

Supplementary text C

In *R. cellullolyticum*, phosphorylated Cph can repress utilization of all soluble/insoluble sugars, indicating transition between unphosphorylated and phosphorylated Cph is likely an efficient and economic way to regulate carbon catabolism (**Figure 2**). Due to the lack of EII complex, sugar transportation is through sugar ABC transporters, which require ATP as energy for transportation. Compared to PTS-mediated sugar transportation, ATP is more precious in *R. cellulolyticum.* To save ATP, previous studies have found that *R. cellulolyticum* possesses some special characteristics, such as preferring to use celloibose instead of glucose (consuming one ATP obtains two glucoses) and using Ppi for fructose-6-phosphate phosphorylation (Park et al., 2019). Therefore, using Ppi for phosphorylation of Cph could be considered as an alternative route for carbon metabolism regulation. When the energy is in deficiency state in the cell (low ATP or glycolysis intermediates), most Cph proteins are under unphosphorylated state (no extra ATP or glycolysis intermediates for phosphorylation) and become a "signal" to induce cells to express carbon catabolic genes (e.g, cellulases and sugar transporters) for energy production and survival. (**Figure 2 & S2**); Continuous high expression of carbon catabolism genes, such as catabolic genes from *cip-cel* operon, is a huge burden for *R. cellulolyticum*. As a result, when the energy is or is about to be at a saturation state (accumulating enough ATPs or glycolysis intermediates for generating ATP), most Cph proteins may be under-phosphorylated (**Table S4**) and become a "signal" to tune down related carbon catabolic genes to avoid over-expression of catabolic genes and cut energy waste (**Figure 2 & S2**).Through prompt transition of phosphorylation states in Cph, *R. cellulolyticum* can have a better competition with other non-cellulose degradation bacteria in nature and make the most of sugars efficiently.

References:

1. Galinier A, Deutscher J. Sophisticated Regulation of Transcriptional Factors by the Bacterial Phosphoenolpyruvate: Sugar Phosphotransferase System. *J Mol Biol* 2017; **429**: 773–789.
2. Deutscher J, Aké FMD, Derkaoui M, Zébré AC, Cao TN, Bouraoui H, et al. The bacterial phosphoenolpyruvate:carbohydrate phosphotransferase system: regulation by protein phosphorylation and phosphorylation-dependent protein-protein interactions. *Microbiol Mol Biol Rev* 2014; **78**: 231–256.
3. Deutscher J, Francke C, Postma PW. How phosphotransferase system-related protein phosphorylation regulates carbohydrate metabolism in bacteria. *Microbiol Mol Biol Rev* 2006; **70**: 939–1031.
4. Fosses A, Maté M, Franche N, Liu N, Denis Y, Borne R, et al. A seven-gene cluster in Ruminiclostridium cellulolyticum is essential for signalization, uptake and catabolism of the degradation products of cellulose hydrolysis. *Biotechnology for Biofuels* 2017;**10: 1-14.**
5. Tobisch S, Zühlke D, Bernhardt J, Stülke J, Hecker M. Role of CcpA in regulation of the central pathways of carbon catabolism in *Bacillus subtilis*. *J Bacteriol* 1999; **181**: 6996–7004.
6. Abranches J, Nascimento MM, Zeng L, Browngardt CM, Wen ZT, Rivera MF, et al. CcpA regulates central metabolism and virulence gene expression in *Streptococcus* mutans. *J Bacteriol* 2008; **190**: 2340–2349.
7. Jones BE, Dossonnet V, Küster E, Hillen W, Josef Deutscher, Klevit RE. Binding of the Catabolite Repressor Protein CcpA to Its DNA Target Is Regulated by Phosphorylation of its Corepressor HPr. *Journal of Biological Chemistry* 1997; **272**: 26530–26535.
8. Schumacher MA, Allen GS, Diel M, Seidel G, Hillen W, Brennan RG. Structural basis for

allosteric control of the transcription regulator CcpA by the phosphoprotein HPr-Ser46-P. *Cell* 2004; **118**: 731–741.

9. Deutscher J, Josef Deutscher, Küster E, Bergstedt U, Charrier V, Hillen W. Protein kinase-dependent HPr/CcpA interaction links glycolytic activity to carbon catabolite repression in Gram-positive bacteria. *Molecular Microbiology* 1995; **15**: 1049–1053
10. Görke B, Stülke J. Carbon catabolite repression in bacteria: many ways to make the most out of nutrients. *Nat Rev Microbiol* 2008; **6**: 613–624.
11. Abdou L, Boileau C, de Philip P, Pagès S, Fiérobe H-P, Tardif C. Transcriptional regulation of the *Clostridium cellulolyticum cip-cel* operon: a complex mechanism involving a catabolite-responsive element. *J Bacteriol* 2008; **190**: 1499–1506.
12. Xu C, Huang R, Teng L, Wang D, Hemme CL, Borovok I, et al. Structure and regulation of the cellulose degradome in *Clostridium cellulolyticum*. *Biotechnol Biofuels* 2013; **6**: 1-15.
13. Ren C, Gu Y, Hu S, Wu Y, Wang P, Yang Y, et al. Identification and inactivation of pleiotropic regulator CcpA to eliminate glucose repression of xylose utilization in *Clostridium acetobutylicum*. *Metab Eng* 2010; **12**: 446–454.
14. Xu C, Huang R, Teng L, Jing X, Hu J, Cui G, et al. Cellulosome stoichiometry in Clostridium cellulolyticum is regulated by selective RNA processing and stabilization. Nat Commun 2015; **6**: 1-13.
15. Nataf Y, Bahari L, Kahel-Raifer H, Borovok I, Lamed R, Bayer EA, et al. *Clostridium thermocellum* cellulosomal genes are regulated by extracytoplasmic polysaccharides via alternative sigma factors. *Proc Natl Acad Sci U S A* 2010; **107**: 18646–18651.
16. Ha J-H, Hauk P, Cho K, Eo Y, Ma X, Stephens K, et al. Evidence of link between quorum sensing and sugar metabolism in *Escherichia coli* revealed via cocrystal structures of LsrK

and HPr. *Sci Adv* 2018; **4**: eaar7063.

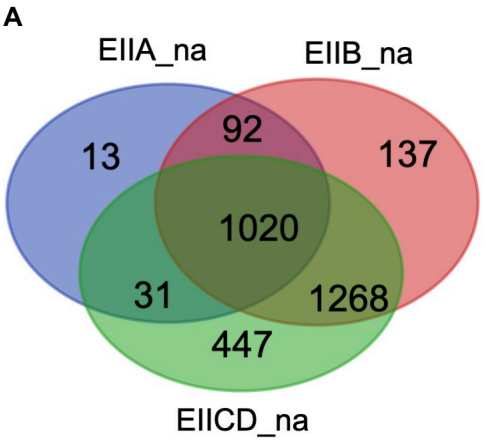
A
EIIA_na
EIIB_na
EIICD_na
13
92
137
1020
31
1268
447

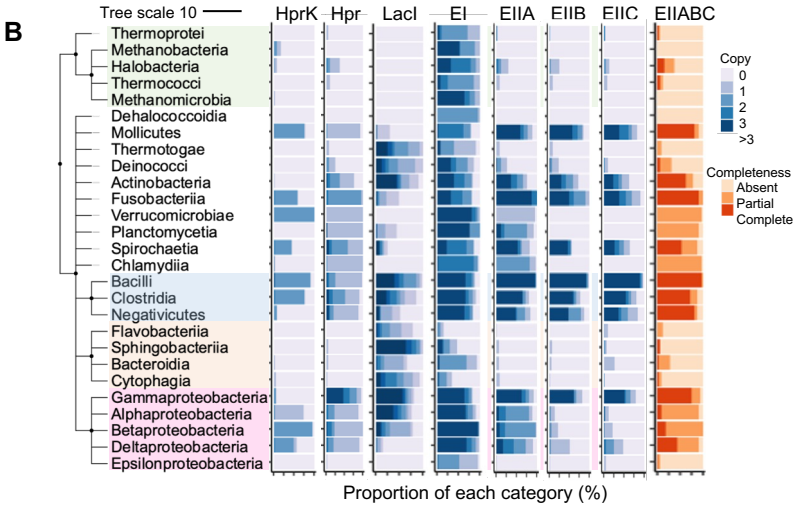
B
Tree scale 10
HprK
Hpr
LacI
EI
EIIA
EIIB
EIIC
EIIABC
Thermoprotei
Methanobacteria
Halobacteria
Thermococci
Methanomicrobia
Dehalococcoidia
Mollicutes
Thermotogae
Deinococci
Actinobacteria
Fusobacteriia
Verrucomicrobiae
Planctomycetia
Spirochaetia
Chlamydiia
Bacilli
Clostridia
Negativicutes
Flavobacteriia
Sphingobacteriia
Bacteroidia
Cytophagia
Gammaproteobacteria
Alphaproteobacteria
Betaproteobacteria
Deltaproteobacteria
Epsilonproteobacteria
Copy
0
1
2
3
>3
Completeness
Absent
Partial
Complete
Proportion of each category (%)

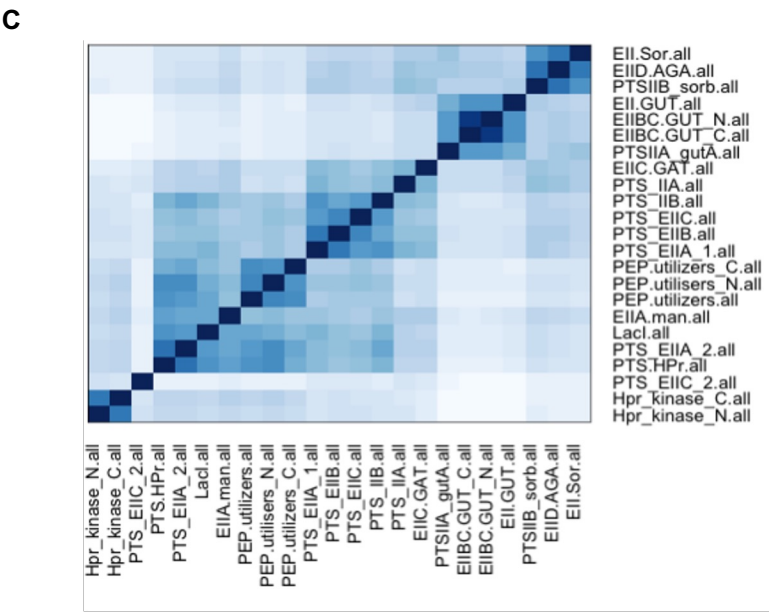
C
EII.Sor.all
EIID.AGA.all
PTSIIB_sorb.all
EII.GUT.all
EIIBC.GUT_N.all
EIIBC.GUT_C.all
PTSIIA_gutA.all
EIIC.GAT.all
PTS_IIA.all
PTS_IIB.all
PTS_EIIC.all
PTS_EIIB.all
PTS_EIIA_1.all
PEP.utilizers_C.all
PEP.utilisers_N.all
PEP.utilizers.all
EIIA.man.all
LacI.all
PTS_EIIA_2.all
PTS.HPr.all
PTS_EIIC_2.all
Hpr_kinase_C.all
Hpr_kinase_N.all
Hpr_kinase_N.all
Hpr_kinase_C.all
PTS_EIIC_2.all
PTS.HPr.all
PTS_EIIA_2.all
LacI.all
EIIA.man.all
PEP_utilizers.all
PEP.utilisers_N.all
PEP.utilizers_C.all
PTS_EIIA_1.all
PTS_EIIB.all
PTS_EIIC.all
PTS_IIB.all
PTS_IIA.all
EIIC.GAT.all
PTSIIA_gutA.all
EIIBC.GUT_C.all
EIIBC.GUT_N.all
EII.GUT.all
PTSIIB_sorb.all
EIID.AGA.all
EII.Sor.all

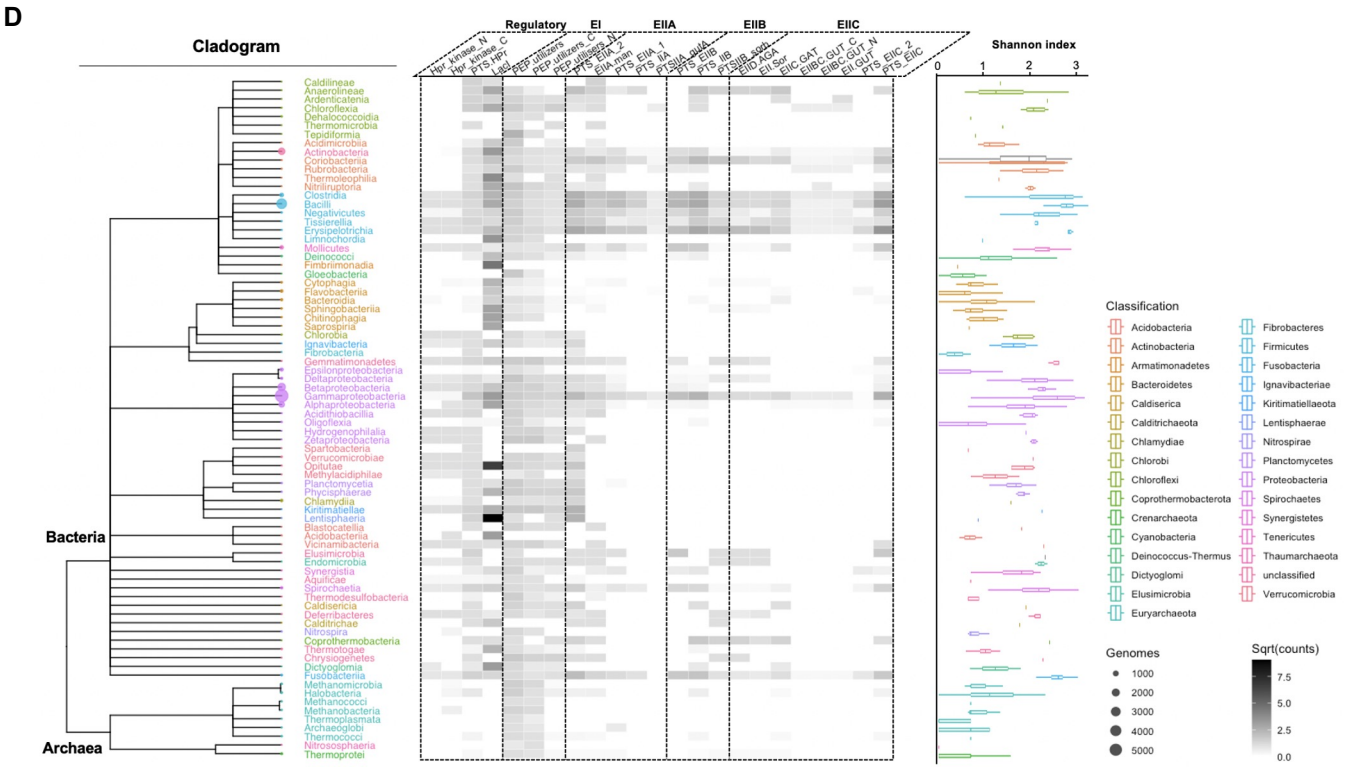
D
Cladogram
Regulatory
EI
EIIA
EIIB
EIIC
Hpr_kinase_N
Hpr_kinase_C
PTS.HPr
LacI
PEP.utilizers
PEP.utilizers_C
PEP.utilizers_N
PTS_EIIA_2
EIIA.man
PTS_EIIA_1
PTS_IIA
PTSIIA_gutA
PTS_EIIB
PTS_IIB
PTSIIB_sorb
EIID.AGA
EII.Sor
EIIC.GAT
EIIBC.GUT_C
EIIBC.GUT_N
EII.GUT
PTS_EIIC_2
PTS_EIIC
Shannon index
0
1
2
3
Bacteria
Archaea
Caldilineae
Anaerolineae
Ardenticatenia
Chloroflexia
Dehalococcoidia
Thermomicrobia
Tepidiformia
Acidimicrobiia
Actinobacteria
Coriobacteriia
Rubrobacteria
Thermoleophilia
Nitriliruptoria
Clostridia
Bacilli
Negativicutes
Tissierellia
Erysipelotrichia
Limnochordia
Mollicutes
Deinococci
Fimbriimonadia
Gloeobacteria
Cytophagia
Flavobacteriia
Bacteroidia
Sphingobacteriia
Chitinophagia
Saprospiria
Chlorobia
Ignavibacteria
Fibrobacteria
Gemmatimonadetes
Epsilonproteobacteria
Deltaproteobacteria
Betaproteobacteria
Gammaproteobacteria
Alphaproteobacteria
Acidithiobacillia
Oligoflexia
Hydrogenophilalia
Zetaproteobacteria
Spartobacteria
Verrucomicrobiae
Opitutae
Methylacidiphilae
Planctomycetia
Phycisphaerae
Chlamydiia
Kiritimatiellae
Lentisphaeria
Blastocatellia
Acidobacteria
Vicinamibacteria
Elusimicrobia
Endomicrobia
Synergistia
Aquificae
Spirochaetia
Thermodesulfobacteria
Caldisericia
Deferribacteres
Calditrichae
Nitrospira
Coprothermobacterota
Thermotogae
Chrysiogenetes
Dictyoglomia
Fusobacteriia
Methanomicrobia
Halobacteria
Methanococci
Methanobacteria
Thermoplasmata
Archaeoglobi
Thermococci
Nitrososphaeria
Thermoprotei
Classification
Acidobacteria
Actinobacteria
Armatimonadetes
Bacteroidetes
Caldiserica
Calditrichaeota
Chlamydiae
Chlorobi
Chloroflexi
Coprothermobacterota
Crenarchaeota
Cyanobacteria
Deinococcus-Thermus
Dictyoglomi
Elusimicrobia
Euryarchaeota
Fibrobacteres
Firmicutes
Fusobacteria
Ignavibacteriae
Kiritimatiellaeota
Lentisphaerae
Nitrospirae
Planctomycetes
Proteobacteria
Spirochaetes
Synergistetes
Tenericutes
Thaumarchaeota
unclassified
Verrucomicrobia
Genomes
1000
2000
3000
4000
5000
Sqrt(counts)
7.5
5.0
2.5
0.0

Figure S1. Distribution and correlation of PTS components in prokaryotes, related to **Figure 1**. **A**,Venn diagram showing the number of species with different configurations in EI and EII components. Strains with singular EI homologs were included; whereas for EIIA/B/C components, strains with either singular or fused architecture were included. **B**, Distribution of PTS components across the phylogenetic tree. For each PTS component, the corresponding plot for each Class represents the percentage of sequenced genomes with a certain copy number or varying in the completeness of EIIABC complex. **C**, Correlation of Jaccard coefficients between all Pfam modules with either singular or fused architecture in prokaryotic genomes. **D**, Heatmap showing the copy number of PTS component homologs in genomes of major Classes.

A

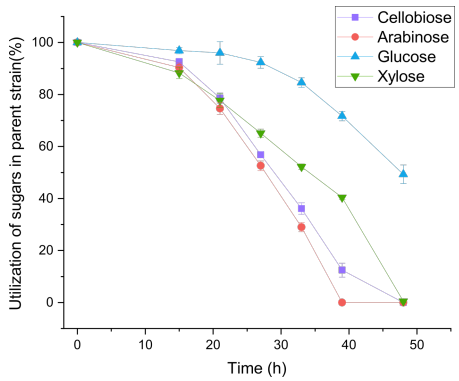

B

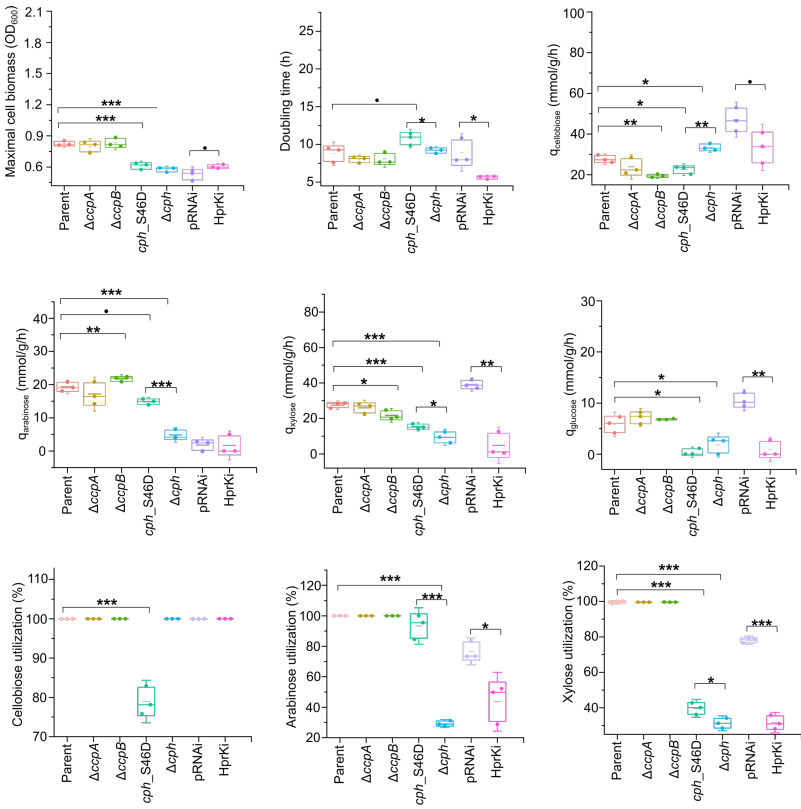

C

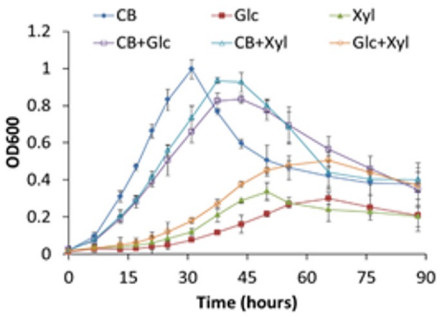

D

Carbon source	Substrate	Growth rate (h^{-1})	Sugar uptake rate (mmol/g/h)
Sole	Cellobiose	0.145	1.88
	Glucose	0.065	4.56
	Xylose	0.071	4.82
Dual	Cellobiose Glucose	0.109	4.37 3.00
	Cellobiose Xylose	0.096	2.84 2.91
	Glucose Xylose	0.071	3.74 6.28

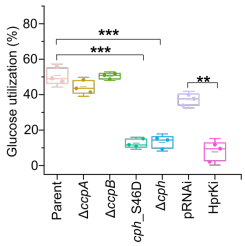

E

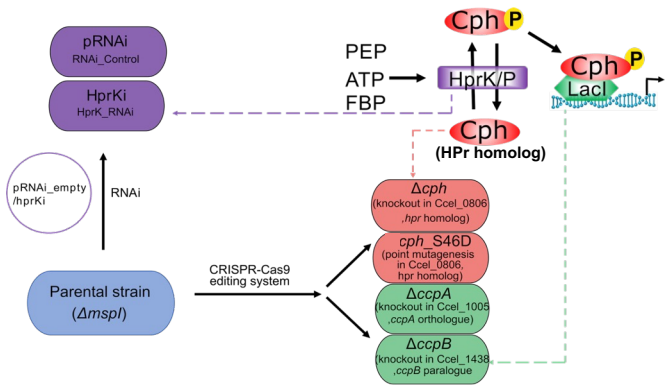

Figure S2. Characterization of metabolic features in *R. cellulolyticum*, related to **Figure 2**. **A,** Utilizations of sugars in the parent strain grown on carbon mixture. **B**, Physiological and metabolic features of the parent strain and PTS mutants grown on different carbon sources. **C**, Growth profiles of *R. cellulolyticum* H10 in the defined VM medium with singular or dual sugars. CB, cellobiose; Glc, glucose; Xyl, xylose. **D**, Measurement of bacterial growth rates and sugar uptake rates under different conditions. **E**, CRISPR-Cas9 genome editing system or RNA interference (RNAi) was used to construct all mutants derived from the parental strain (Δ*mspI*).

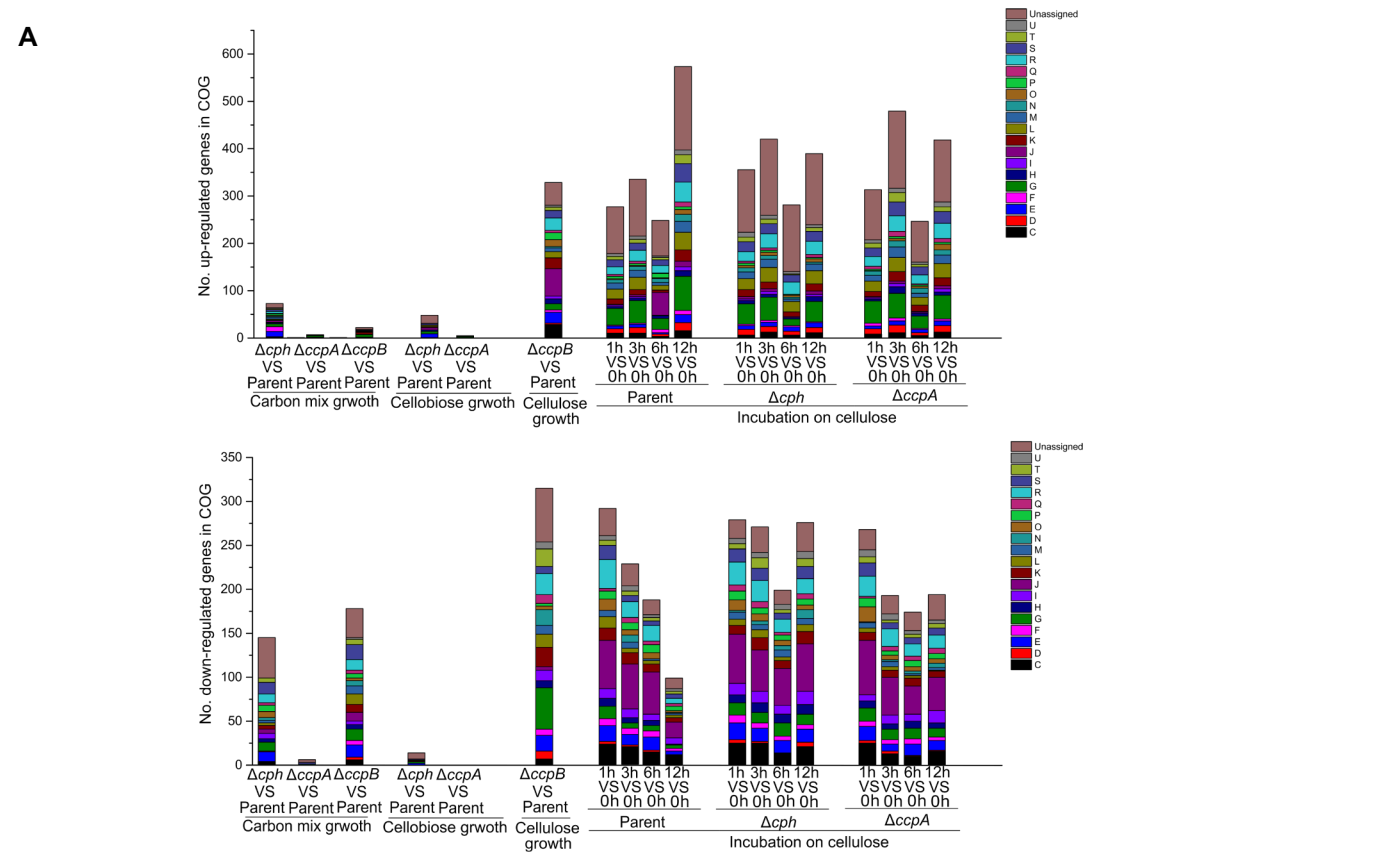
A
No. up-regulated genes in COG
No. down-regulated genes in COG
Unassigned
U
T
S
R
Q
P
O
N
M
L
K
J
I
H
G
F
E
D
C
Δcph VS Parent
ΔccpA VS Parent
ΔccpB VS Parent
Δcph VS Parent
ΔccpA VS Parent
ΔccpB VS Parent
1h VS 0h
3h VS 0h
6h VS 0h
12h VS 0h
Carbon mix grwoth
Cellobiose grwoth
Cellulose growth
Parent
Δcph
ΔccpA
Incubation on cellulose

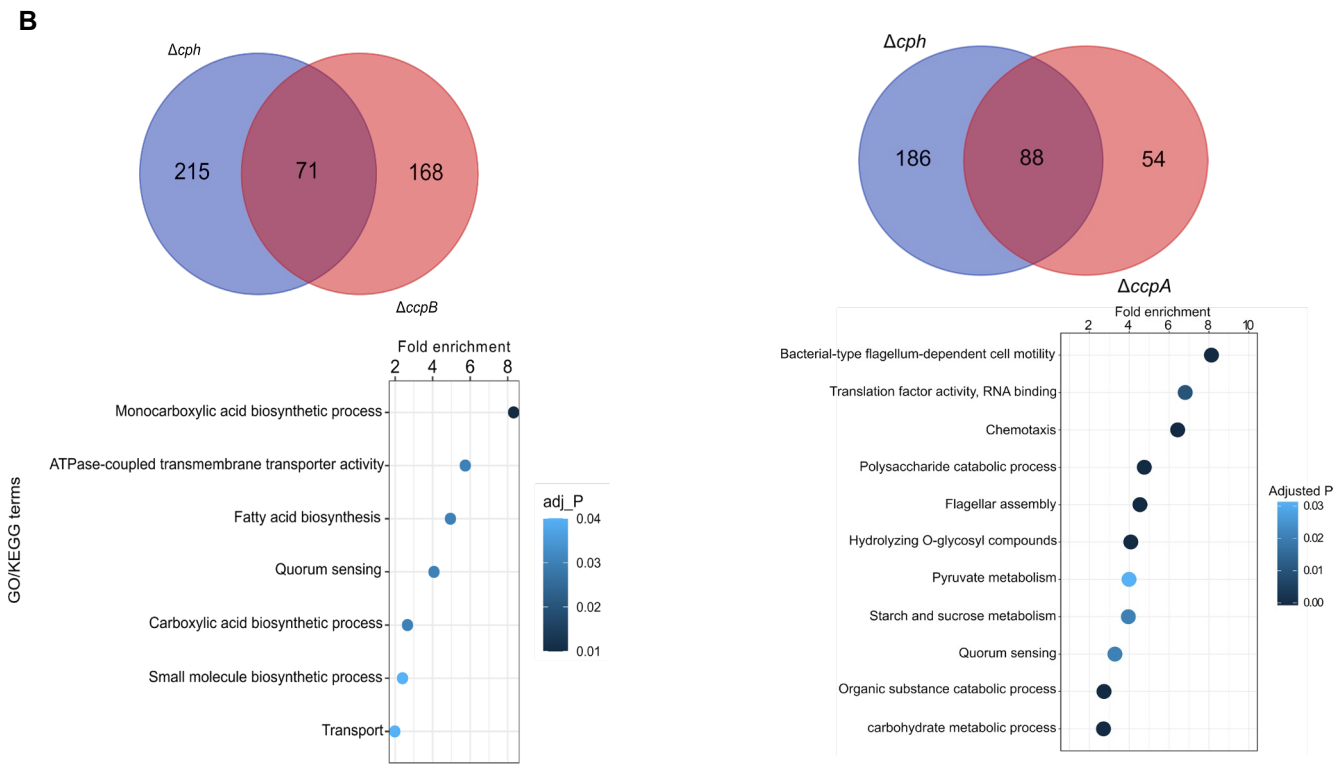
B
Δcph
215
71
168
ΔccpB
Δcph
186
88
54
ΔccpA
GO/KEGG terms
Fold enrichment
Monocarboxylic acid biosynthetic process
ATPase-coupled transmembrane transporter activity
Fatty acid biosynthesis
Quorum sensing
Carboxylic acid biosynthetic process
Small molecule biosynthetic process
Transport
adj_P
Bacterial-type flagellum-dependent cell motility
Translation factor activity, RNA binding
Chemotaxis
Polysaccharide catabolic process
Flagellar assembly
Hydrolyzing O-glycosyl compounds
Pyruvate metabolism
Starch and sucrose metabolism
Quorum sensing
Organic substance catabolic process
carbohydrate metabolic process
Adjusted P

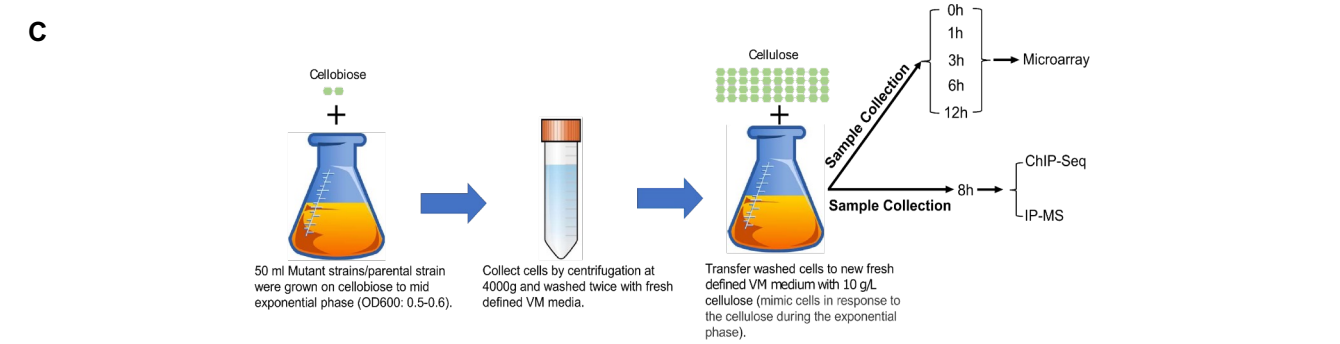
C
Cellobiose
Cellulose
Sample Collection
0h
1h
3h
6h
12h
Microarray
8h
ChIP-Seq
IP-MS
50 ml Mutant strains/parental strain were grown on cellobiose to mid exponential phase (OD600: 0.5-0.6).
Collect cells by centrifugation at 4000g and washed twice with fresh defined VM media.
Transfer washed cells to new fresh defined VM medium with 10 g/L cellulose (mimic cells in response to the cellulose during the exponential phase).

Figure S3. Transcriptional analysis in *R. cellulolyticum* grown on carbon mixture or cellulose, related to **Figure 3.** **A**, The number of upregulated and downregulated DEGs in COG across mutants grown on cellobiose, carbon mix or cellulose. All strains were compared to the parental strain (Δ*mspI*) or its time zero to count DEGs ($p<0.01$ and $log2|FC|>2$). [D] Cell cycle control, cell division, chromosome partitioning; [M] Cell wall/membrane/envelope biogenesis; [N] Cell motility; [O] Post-translational modification, protein turnover, and chaperones; [T] Signal transduction mechanisms; [U] Intracellular trafficking, secretion, and vesicular transport; [V] Defense mechanisms; [W] Extracellular structures; [Y] Nuclear structure; [Z] Cytoskeleton; [A] RNA processing and modification; [B] Chromatin structure and dynamics; [J] Translation, ribosomal structure and biogenesis; [K] Transcription; [L] Replication, recombination and repair; [C] Energy production and conversion; [E] Amino acid transport and metabolism; [F] Nucleotide transport and metabolism; [G] Carbohydrate transport and metabolism; [H] Coenzyme transport and metabolism; [I] Lipid transport and metabolism; [P] Inorganic ion transport and metabolism; [Q] Secondary metabolites biosynthesis, transport, and catabolism; [R] General function prediction only; [S] Function unknown. **B**, Venn diagram for DEGs of Δ*cph* and Δ*ccpB* on carbon mixture and GO enrichment analysis of shared DEGs between Δ*cph* and Δ*ccpB* on carboon mixture (*left*); Venn diagram for DEGs in Δ*cph* and Δ*ccpA* compared to parental strain at 12h of the incubation experiment and GO enrichment analysis of shared DEGs between Δ*cph* and Δ*ccpA* on cellulose (*Right*). **C**, the designing of the incubation experiment used for the microarray (response to cellulose for Δ*ccpA* and Δ*cph*), ChIP-seq and IP-MS experiments.

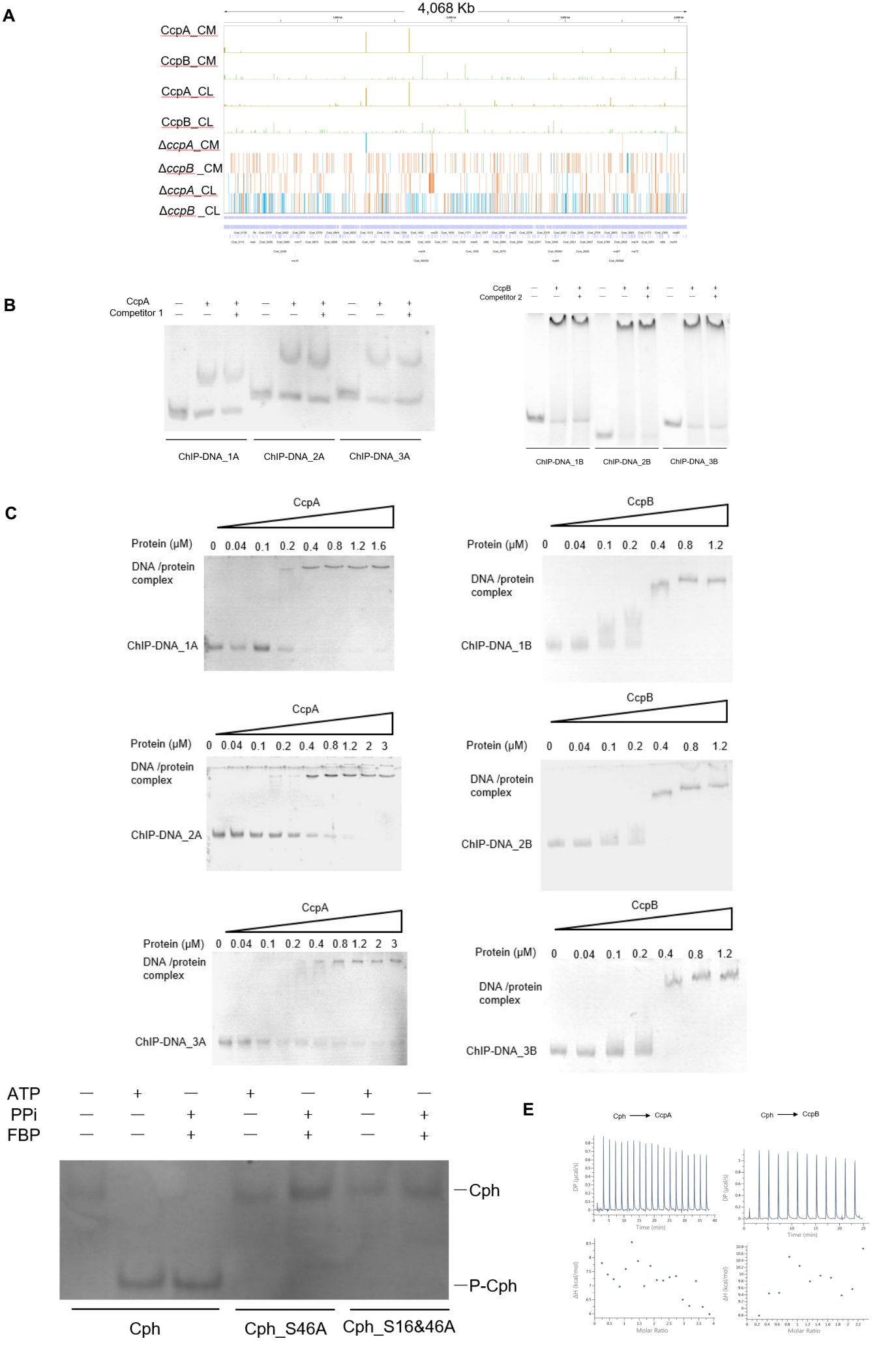
A
4,068 Kb
CcpA_CM
CcpB_CM
CcpA_CL
CcpB_CL
ΔccpA_CM
ΔccpB _CM
ΔccpA_CL
ΔccpB _CL
B
CcpA
Competitor 1
ChIP-DNA_1A
ChIP-DNA_2A
ChIP-DNA_3A
CcpB
Competitor 2
ChIP-DNA_1B
ChIP-DNA_2B
ChIP-DNA_3B
C
CcpA
Protein (μM) 0 0.04 0.1 0.2 0.4 0.8 1.2 1.6
DNA /protein complex
ChIP-DNA_1A
CcpB
Protein (μM) 0 0.04 0.1 0.2 0.4 0.8 1.2
DNA /protein complex
ChIP-DNA_1B
CcpA
Protein (μM) 0 0.04 0.1 0.2 0.4 0.8 1.2 2 3
DNA /protein complex
ChIP-DNA_2A
CcpB
Protein (μM) 0 0.04 0.1 0.2 0.4 0.8 1.2
DNA /protein complex
ChIP-DNA_2B
CcpA
Protein (μM) 0 0.04 0.1 0.2 0.4 0.8 1.2 2 3
DNA /protein complex
ChIP-DNA_3A
CcpB
Protein (μM) 0 0.04 0.1 0.2 0.4 0.8 1.2
DNA /protein complex
ChIP-DNA_3B
D
ATP
PPi
FBP
Cph
P-Cph
Cph
Cph_S46A
Cph_S16&46A
E
Cph → CcpA
Cph → CcpB
DP (μcal/s)
Time (min)
ΔH (kcal/mol)
Molar Ratio

Figure S4. Biochemical characterization of CcpA, CcpB and Cph in *R. cellulolyticum*, related to **Figure 4**. **A,** Integration of transcriptomic responses and DNA binding profiles for *R.cellulolyticum* CcpA and CcpB. The transcriptomic responses (heatmap) in Δ*ccpA* and Δ*ccpB* grown on carbon mixture (CM) or cellulose (CL) were based on the microarray analysis and the DNA binding profiles (bar graph) of CcpA and CcpB were determined by ChIP-seq (see M&M and Table S3 for details). Blue, up-regulated DEGs; Orange, down-regulated DEGs. Genes potentially directly regulated by CcpA or CcpB are listed in Table S4. **B**, Competition experiments to confirm the binding specificity of Ccp proteins. The Electrophoretic mobility shift assays is performed with CcpA or CcpB and competitor DNA sequences. Competitor 1 DNA is CcpB-binding consensus oligonucleotide (forward 5'-TATAATGGGAACGTTCCCATGTTG-3' , reverse 5'- CAACATGGGAACGTTCCCATTATA-3') and competitor 2 DNA is CcpA binding consensus oligonucleotide (forward 5'-TATAACGAATCGTTTTGTGTTG-3', reverse 5' -CAACACAAAACGATTCGTTATA-3'). Competitor 1 and Competitor 2 were added at a 625-fold molar excess. **C,** Validation of binding between CcpA or CcpB and select DNA sequences identified by ChIP-Seq. The selected DNA sequences were the top three most enriched peaks identified by ChIP-seq for CcpA or CcpB (Table S5). The electrophoretic mobility shift assay was used to confirm binding between protein and DNA. **D**, Native-PAGE gel verified that Ppi and FBP were co-provided for Hprk in phosphorylating Cph. The phosphorylation site in Cph (S46) was further confirmed by LC-MS/MS (Table S4). **E,** Unphosphorylated Cph cannot interact with the CcpA or the CcpB. Raw isothermal titration calorimetry data (*upper*) and derived binding isotherm plotted *versus* the molar ratio of titrant which was fit using a one-site model (*lower*) for Cph (titrant) into CcpA or CcpB (sample).

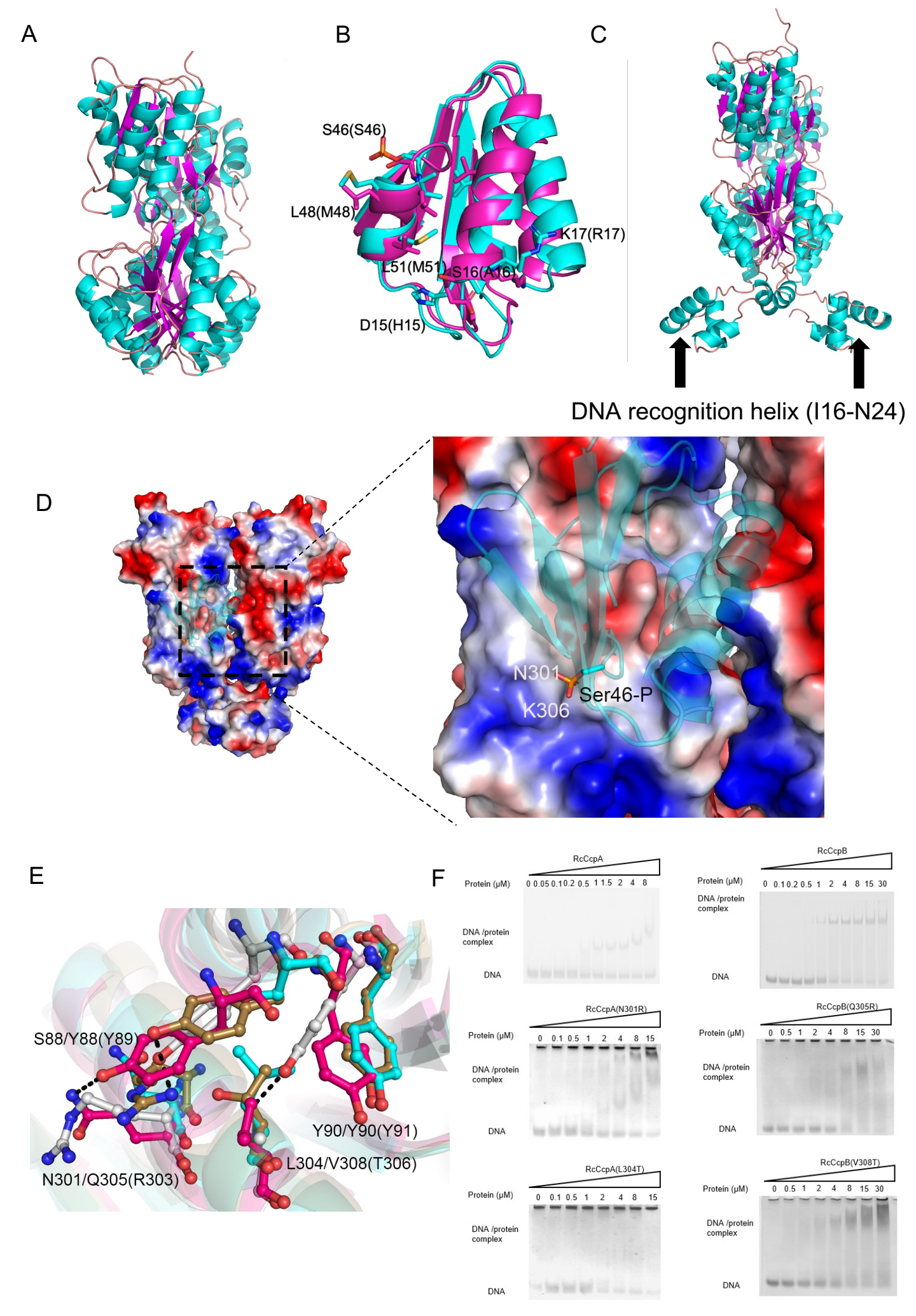
A
B
S46(S46)
L48(M48)
K17(R17)
L51(M51)
S16(A16)
D15(H15)
C
DNA recognition helix (I16-N24)
D
N301
Ser46-P
K306
E
S88/Y88(Y89)
Y90/Y90(Y91)
L304/V308(T306)
N301/Q305(R303)
F
RcCcpA
Protein (μM)
0 0.05 0.1 0.2 0.5 1 1.5 2 4 8
DNA /protein complex
DNA
RcCcpB
Protein (μM)
0 0.1 0.2 0.5 1 2 4 8 15 30
DNA /protein complex
DNA
RcCcpA(N301R)
Protein (μM)
0 0.1 0.5 1 2 4 8 15
DNA /protein complex
DNA
RcCcpB(Q305R)
Protein (μM)
0 0.5 1 2 4 8 15 30
DNA /protein complex
DNA
RcCcpA(L304T)
Protein (μM)
0 0.1 0.5 1 2 4 8 15
DNA /protein complex
DNA
RcCcpB(V308T)
Protein (μM)
0 0.5 1 2 4 8 15 30
DNA /protein complex
DNA

Figure S5. Structure analysis of CcpA, CcpB and Cph proteins in *R. cellulolyticum* and DNA binding affinities for RcCcpA and RcCcpA mutants, related to **Figure 5**. **A,** The overall structure of CcpB dimer from *R. cellulolyticum.* **B,** Supposition of the Cph structure (magenta) onto the HPr structure (cyan). The residues responsible for interacting with CcpA were shown in sticks and labelled. The residue labels for HPr were shown in parentheses. **C,** The overall structure of the CcpA (predicted by AlphaFold2) from *R. cellulolyticum*. The predicted DNA-recognition helices of RcCcpA were labelled. **D**, Surface potential of the predicted CcpA dimer from *R. cellulolyticum* (RcCcpA). The RcCcpA dimer was superimposed to the BmCcpA dimer of BmCcpA-HprSer46P complex and the structure of Hpr and Cph was shown in a cyan cartoon representation, with the Ser46P shown in sticks. The equivalent HprSer46P-interacting residues in RcCcpA residues were shown in sticks and labelled. **E**, Hydrogen bonding network essential for CcpA conformational switching in *B. megaterium* apo-CcpA (white), CcpAHprSer46P complex (yellow), R. cellulolyticum apo-CcpB (magenta) and predicted apo-CcpA structures (cyan). The residue labels for RcCcpA were shown first and the residues labels for BmCcpA were shown in parentheses. **F**, DNA binding affinities for RcCcpA and RcCcpA mutant proteins**.** Electrophoretic mobility shift assays with purified proteins and select DNA sequences identified by CHIP-Seq. DNA used for RcCcpA or RcCcpA mutant proteins are 5'-TATAACGAATCGTTTTGTGTTG-3'; DNA used for RcCcpB or RcCcpB mutant proteins are 5'-CTCAATGTTAACGGTTCCATTTAC-3'.